JOURNAL OF GEOPHYSICAL RESEARCH, VOL. 97, NO. B2, PAGES 2085–2093, FEBRUARY 10, 1992

# Analytical Models for Flow Through Obstructed Domains

ANDREW R. PIGGOTT[1]

*Dowell Schlumberger Incorporated, Tulsa, Oklahoma*

DEREK ELSWORTH

*Department of Mineral Engineering, Pennsylvania State University, University Park*

The effects of low- or zero-conductivity inclusions on flow through two- and three-dimensional domains are represented using an analogy to percolation theory. Here, the term flow refers to the analogous processes of fluid, electrical current, and heat conduction. Mapping functions are derived from renormalization group models as a solution to the percolation analogy. These functions relate the extent to which a domain is obstructed to the probability that the domain is conductive and to the bulk conductivity of the domain. Stochastic methods are used to define a relation between the proportion of a domain which is isolated from flow and the proportion which is obstructed. A description of the influence of the scale of the obstructions, relative to that of the domain, is inherent in the formulation. Data obtained from numerical and electrical analogues are used to verify the mapping functions and assess the limitations of the representation.

## INTRODUCTION

A useful description of a geologic process relies upon an appropriate representation of the associated physical properties including a description of the spatial variability of these properties. However, it is often not feasible to explicitly represent the variability of properties at the scale of relevant processes. This is particularly true in cases where the spatial distribution of properties is known in insufficient detail to form a deterministic description of the system. Under these conditions, the use of equivalent properties which reflect the variability of the actual properties may be an appropriate alternative. By way of illustration, the case of fluid flow through rough-walled rock fractures is briefly considered in the following.

Experimental studies indicate that rough-walled fractures are characterized by spatially variable aperture [*Gentier and Billaux*, 1989] and by nonconductive inclusions resulting from fracture surface-to-surface contact [*Pyrak-Nolte et al.*, 1987]. In simulating flow through a fracture, it is reasonable to assign a conductivity of zero to the areas of surface-to-surface contact. This representation requires the specification of no-flow boundary conditions to describe the perimeter of the areas of contact and could lead to a demanding discretization and numerical simulation exercise. Rather than resorting to an analysis in which fracture aperture is represented in a deterministic sense, it is possible to base predictions on the relative abundance of contact area and on the characteristic aperture of the open portions of the fracture. It is fortuitous that the behavior of such systems is often relatively insensitive to the precise details of the distribution of properties and that a statistical estimate of behavior will suffice.

This paper introduces a method of determining the conductive properties of domains characterized by low- or zero-conductivity flow obstructions. Although the previous example addressed the specific case of fluid flow, the developments are equally applicable to the analogous processes of electrical current and heat conduction. For clarity, a consistent terminology is adopted. Formulations are presented for both two- and three-dimensional flow, and therefore the term domain denotes a two- or three-dimensional flow domain. The term conductivity refers to hydraulic, electrical, and thermal conductivity according to the flow process under consideration. Hydraulic conductivity takes on the specific definition of transmissivity for two-dimensional flow. Flow obstructions are idealized as nonconductive inclusions.

The conductivity distribution model adopted herein regards domains as assemblies of discrete equidimensional microscale elements of finite dimension and constant conductivity. Using the terminology of geostatistics, these distributions are perfectly correlated at scales up to that of the element dimension and are uncorrelated at larger scales. A proportion of the elements, distributed at random, are assumed to be nonconductive. The microscale distribution of obstructions and conductivity is assumed to be isotropic and leads to isotropic macroscale behavior. These assumptions are restrictive and applicable to only a subset of geologic media. However, the ability to derive analytical models, and the insight gained from the models, warrant acceptance of these limitations.

This paper begins by offering percolation theory as an analogue to the process of flow through obstructed domains. Models derived from renormalization group theory are then developed as a solution to the percolation analogy. Finally, stochastic modelling exercises are undertaken in order to verify the results predicted by the models and assess the limitations of the approach.

## FLOW THROUGH OBSTRUCTED DOMAINS

The influence of obstructions on flow may be represented through an analogy to percolation theory, which describes the conductive behavior and properties of disordered systems of conducting and nonconducting elements. Introductions to percolation theory are presented by *Shante and Kirkpatrick* [1971] and *Kirkpatrick* [1973] to which the reader is referred for a comprehensive description of the approach. Central to percolation theory is the definition of a critical or threshold density of nonconductive elements that separates conductive and nonconductive arrangements of the elements. Subsequent to this is a relation between the density of nonconductive elements and the

[1] Now at National Water Research Institute, Burlington, Ontario.



Paper number 91JB02641.
0148-0227/92/91JB-02641$05.00

overall or bulk conductivity of the arrangements. Clearly, the concepts of percolation theory are allied with the issues addressed in this paper.

A number of applications of percolation theory in hydrogeology and geomechanics have been reported. Mechanical and transport aspects of fracture system connectivity have been investigated by *Madden* [1976], *Chelidze* [1982], *Dienes* [1982], *Charlaix et al.* [1984], *de Marsily* [1985], *Wilke et al.* [1985], *Robinson* [1987], *Gueguen and Dienes* [1989], and *Hestir and Long* [1990]. The transport properties of porous media have been examined by *Shankland and Waff* [1974] and *Golden* [1980]. These studies demonstrate the utility of percolation theory as a means of quantifying the behavior of randomly structured geologic media.

Analytical models based on renormalization group theory are well suited to the description of critical processes such as percolation. The fundamental operation involved in the application of renormalization group theory is the derivation of mapping functions which translate characteristics or properties at one scale to a second, physically larger, scale. The term mapping function is used to denote the fact that discrete, rather than continuous, changes in scale are represented. Mapping functions are derived by grouping individual elements at the first scale into an assembled model at the second and larger scale and by evaluating the properties of the model based on the properties of the individual elements. This scaling process is illustrated for two- and three-dimensional systems in Figure 1. The behavior of a large-scale system (e.g., $i = 3$) is described by the individually conductive or nonconductive behavior of the component cells ($i = 0$). Renormalization group theory is an attractive approach because of this explicit description of the scaling process.

A limited number of applications of renormalization group theory in geomechanics have been reported. *Allègre et al.* [1982] and *Turcotte* [1986] used a renormalization group model to describe the fracture and fragmentation of rock. *Madden* [1983] applied a renormalization group approach to the analysis of the conductivity and mechanical integrity of fractured rock. A renormalization group treatment of the stick-slip behavior of faults is presented by *Smalley et al.* [1985]. The approach presented in this paper follows from that applied by *Allègre et al.* [1982] and *Turcotte* [1986].

Figure 1 shows the renormalization group models adopted in this study. The representation begins with nondivisible zero order cells ($i = 0$). Four and eight zero order cells are assembled into a first order cell ($i = 1$) in the two- and three-dimensional models, respectively. First order cells are then assembled into second order cells ($i = 2$) and second order cells into third order cells ($i = 3$). The process is repeatedly applied, and ultimately the contribution of a single zero order cell becomes negligible with respect to the whole. The properties of the whole are, however, entirely a function of those of the zero order cells. The models shown in Figure 1 are not unique and could have been based on, for example, the assembly of nine and 27 $i$ order cells into $i + 1$ order cells. Preliminary studies indicate that the performance of the models is rather insensitive to the form of the models; that is, the behaviors predicted by the models shown in Figure 1 do not differ significantly from those predicted by models assembled from nine and 27 $i$ order cells. This, and the substantial complications associated with more detailed models, supports the use of the models shown in Figure 1. Models based on different cell geometries (e.g., triangular cells) may yield significantly different results.

The formulation of the renormalization group models is based on the assumption that each $i$ order cell is either conductive or nonconductive and, if conductive, has a characteristic conductivity. Operational definitions of the terms conductive, nonconductive, and characteristic conductivity are deferred to a subsequent section of this paper. The probability that an $i$ order cell is nonconductive is denoted as $p_i$, and the characteristic conductivity of the cell is $K_i$. When $i$ order cells are assembled into an $i + 1$ order cell, the probability that the resulting cell is nonconductive, $p_{i+1}$, and the conductivity of the cell, $K_{i+1}$, are derived from the corresponding values for $i$ order cells.

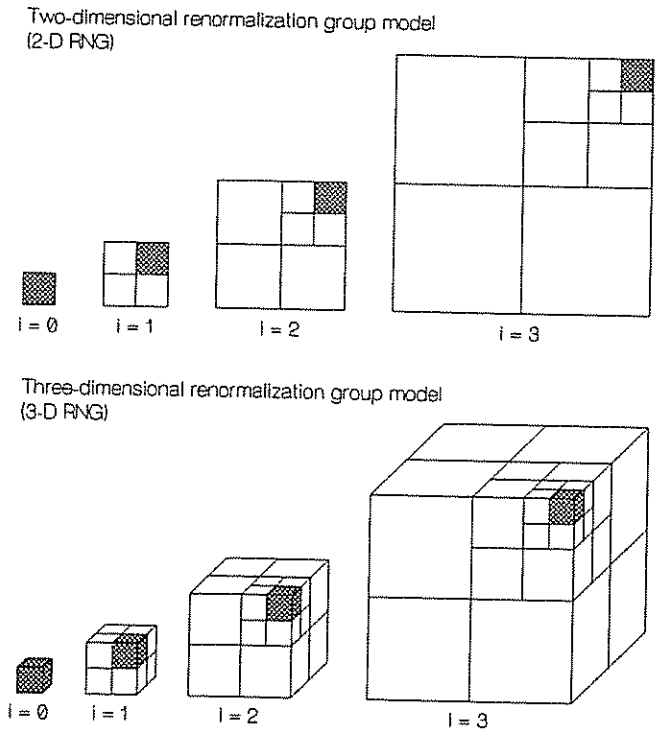


Fig. 1. Illustration of the renormalization group models.

*Probability Mapping*

Table 1 shows the number of arrangements of $i$ order cells which yield nonconductive $i + 1$ order cells, and the probability of each of these arrangements, as a function of the number of nonconductive $i$ order cells. For example, for the two-dimensional model there are four arrangements of two nonconductive and two conductive $i$ order cells which result in nonconductive $i + 1$ order cells. The probability of each of these arrangements is $p_i^2(1 - p_i)^2$. The probability that an $i + 1$ order cell is nonconductive is the sum of the probabilities of all nonconductive arrangements and, for the two-dimensional model, is given by

$$p_{i+1} = 4p_i^2(1-p_i)^2 + 4p_i^3(1-p_i) + p_i^4 = p_i^4 - 4p_i^3 + 4p_i^2 . \quad (1)$$

The three-dimensional equivalent of (1) is

$$p_{i+1} = 16p_i^4(1-p_i)^4 + 32p_i^5(1-p_i)^3 + 24p_i^6(1-p_i)^2 + 8p_i^7(1-p_i) + p_i^8 = p_i^8 - 8p_i^7 + 24p_i^6 - 32p_i^5 + 16p_i^4 . \quad (2)$$

The fixed points of (1) and (2) are defined as those values of $p_i$ which satisfy the condition

$$p_{i+1} = p_i . \quad (3)$$

TABLE 1. Number and Probability of Nonconductive $i + 1$ Order Arrangements of $i$ Order Cells as a Function of the Number of Nonconductive $i$ Order Cells

| Number of Nonconductive $i$ Order Cells | Number of Nonconductive $i + 1$ Order Arrangements | | Probability of Each Nonconductive $i + 1$ Order Arrangement | |
|---|---|---|---|---|
| | 2-D | 3-D | 2-D | 3-D |
| 0 | 0 | 0 | $(1-p_i)^4$ | $(1-p_i)^8$ |
| 1 | 0 | 0 | $p_i(1-p_i)^3$ | $p_i(1-p_i)^7$ |
| 2 | 4 | 0 | $p_i^2(1-p_i)^2$ | $p_i^2(1-p_i)^6$ |
| 3 | 4 | 0 | $p_i^3(1-p_i)$ | $p_i^3(1-p_i)^5$ |
| 4 | 1 | 16 | $p_i^4$ | $p_i^4(1-p_i)^4$ |
| 5 | | 32 | | $p_i^5(1-p_i)^3$ |
| 6 | | 24 | | $p_i^6(1-p_i)^2$ |
| 7 | | 8 | | $p_i^7(1-p_i)$ |
| 8 | | 1 | | $p_i^8$ |

Models are two-dimensional (2-D) and three-dimensional (3-D).

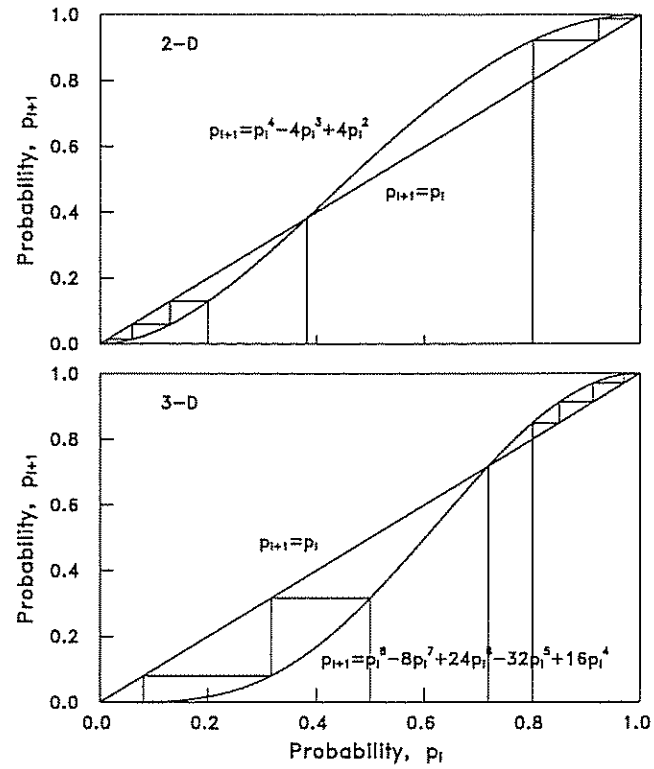


Fig. 2. Probability mapping functions relating the probabilities that $i$ and $i + 1$ order cells are nonconductive for two-dimensional (2-D) (upper) and three-dimensional (3-D) (lower) domains. Trajectories illustrate iterations of the mapping functions.

Equation (1) has valid fixed points (i.e., in the range of zero to unity) located at $p_i = 0$, 0.382, and 1, while (2) has fixed points located at $p_i = 0$, 0.718, and 1 (the values 0.382 and 0.718 are approximations of the true irrational values). Fixed points are classified as stable and unstable, where stable fixed points are characterized by [*Atkinson*, 1978]

$$\left| \frac{dp_{i+1}}{dp_i} \right| < 1 . \tag{4}$$

The derivative of (1) is

$$\frac{dp_{i+1}}{dp_i} = 4p_i^3 - 12p_i^2 + 8p_i \tag{5}$$

and has a magnitude of zero at the fixed point values of zero and unity and a magnitude of 1.528 at the fixed point value of 0.382. Similarly, the derivative of (2) is

$$\frac{dp_{i+1}}{dp_i} = 8p_i^7 - 56p_i^6 + 144p_i^5 - 160p_i^4 + 64p_i^3 \tag{6}$$

and has magnitude of zero at the fixed point values of zero and unity and a magnitude of 1.759 at the fixed point value of 0.718. Clearly, the fixed points located at 0.382 and 0.718 are unstable. The stability of a fixed point describes the tendency of an initial estimate of the fixed point value to converge to the true value in the case of stable fixed points and to diverge in the case of unstable fixed points.

Equations (1) and (3) and (2) and (3) are shown in Figure 2, where the fixed points are apparent as the intersection of the respective equations. The stability of the fixed points is illustrated by the trajectories which graphically demonstrate iterations of the equations; that is, calculating $p_1$ from $p_o$, $p_2$ from $p_1$, etcetera. Any trajectory which initiates at a probability less than that corresponding to the central unstable fixed point is ultimately attracted to the stable fixed point at zero. Trajectories initiating at probabilities greater than that corresponding to the unstable fixed point are attracted to the stable fixed point at unity. Only if a trajectory initiates at precisely the unstable fixed point value will it fail to converge to one of the stable fixed points.

Figure 3 shows the results of repeated applications of the probability mapping functions, (1) and (2). The relation between $p_i$ and $p_o$ converges to a step function centered at the unstable fixed point as the number of iterations approaches infinity. This suggests that infinitely large two- and three-dimensional arrangements of zero order cells will be conductive for zero order probabilities less than 0.382 and 0.718, respectively. For zero order probabilities greater than these values, the corresponding arrangements will be nonconductive. Returning to the percolation analogy, the unstable fixed point values of 0.382 and 0.718 are estimates of the critical probabilities, $p_c$, for the two-dimensional site percolation problem on a square lattice and the three-dimensional site percolation problem on a cubic lattice.

Also shown in Figure 3 are the results of stochastic experiments performed using two- and three-dimensional finite difference based numerical models. The modelling procedure begins by generating a two- or three-dimensional array of sites with each site assigned a conductivity of unity. Some of the sites are then selected at random and assigned a conductivity of zero. The number of nonconductive sites is calculated as the product of the total number of sites and the specified proportion of nonconductive sites, $p_o$. The total flow through the system, if any, is then evaluated. The geometry of a typical 16 × 16 two-dimensional array of sites with $p_o = 0.2$ is shown in Figure 4. A more detailed description of this modelling procedure is presented by *Piggott* [1990]. The probability that an array is nonconductive is estimated as the ratio of the number of nonconductive arrays encountered to the total number of arrays generated. It is assumed in applying this

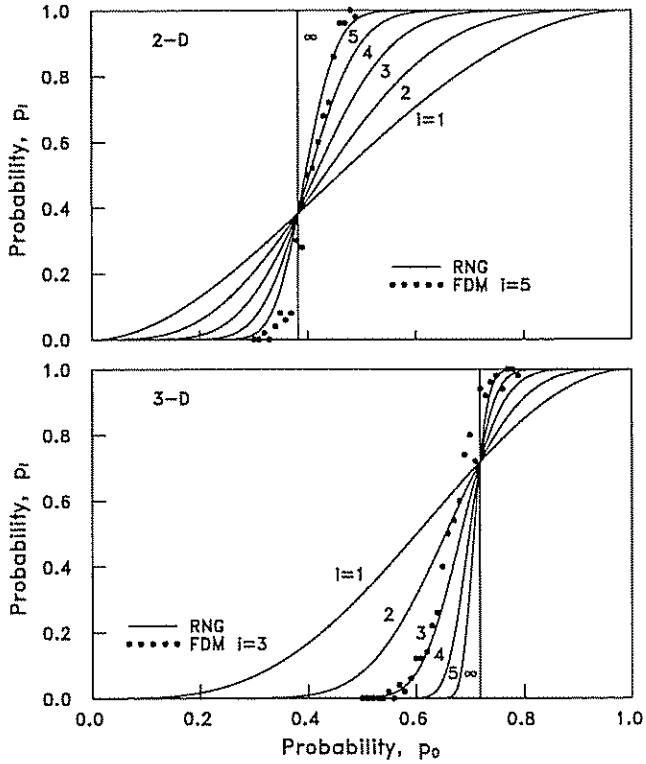


Fig. 3. Iterations of the probability mapping functions. The probability mapping functions (RNG) are compared to data derived from the numerical models (FDM).

procedure that the results for $32 \times 32$ arrays of sites can be compared to the two-dimensional probability mapping for $i = 5$ (i.e., $2^5 = 32$) and that the results for $8 \times 8 \times 8$ arrays can be compared to the three-dimensional probability mapping for $i = 3$ (i.e., $2^3 = 8$). The points shown in Figure 3 correspond to a total of 50 runs for each value of $p_o$. The probability mapping functions and numerical model results illustrate favorable agreement although the numerical results may suggest a slightly larger critical probability than the two-dimensional mapping and a slightly smaller critical probability than the three-dimensional mapping. In a review of documented values, *Sykes and Essam* [1964] reported critical probabilities of the order of 0.41-0.42 and 0.68-0.69 for two- and three-dimensional problems, respectively. These values substantiate the observed discrepancy between the probability mapping and experimental results. The accuracy of the probability mapping is, however, adequate for the purpose of the developments presented in this paper.

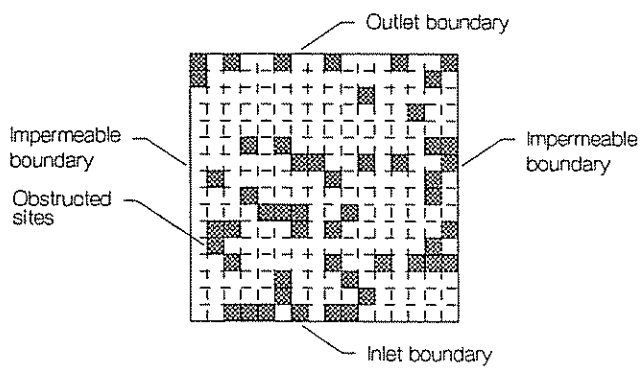


Fig. 4. Illustration of a $16 \times 16$ array of sites with $p_o = 0.2$. The direction of flow is from bottom to top. Obstructed sites are shaded.

*Isolation Mapping*

The probability that a zero order cell is nonconductive is directly analogous to the proportion of the domain which is obstructed. It is conceivable that conductive portions of a domain may be isolated from the active flow domain as the result of the distribution of obstructions; that is, these regions may be entirely surrounded by obstructions. An isolated zone neither conducts during steady state flow nor provides storage during transient flow. No means of estimating the extent of isolation via the renormalization group models were identified so, as an alternative, stochastic studies were performed using the numerical models. The numerical models regard sites which are not connected to both the inlet and outlet boundaries via conductive sites to be isolated. The probability that a site is isolated, $p'_i$, corresponding to the probability that a zero order site is nonconductive, $p_o$, is obtained by dividing the observed number of isolated sites by the total number of sites. Figure 5 shows the results of applying this approach to various two- and three-dimensional arrays where the points reflect the average value of $p'_i$ for 20 runs. The results appear to converge with scale towards the function

$$\lim_{i \to \infty} p'_i = \begin{cases} p_o & \text{for } p_o < p_c \\ 1 & \text{for } p_o > p_c \end{cases} \tag{7}$$

which is also shown in Figure 5. This implies that the entire flow domain remains connected until $p_o$ exceeds $p_c$ at which point the entire domain becomes isolated.

For the particular case of fluid flow, the extent to which a domain retards solute transport by advection is, roughly speaking, a function of the hydraulically connected volume of the domain.

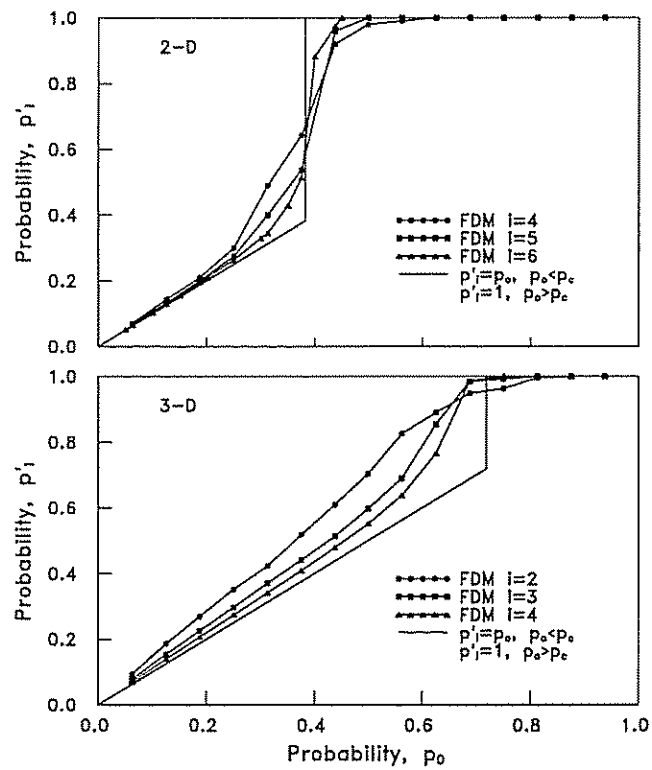


Fig. 5. Variation of the probability that an $i$ order cell is isolated with the probability that a zero order cell is nonconductive.

The fact that the entire unobstructed volume of a conductive domain is connected implies that the total volume of the domain is available to retard solute transport.

*Conductivity Mapping*

Equations (1) and (2) relate the probabilities that $i$ and $i + 1$ order cells are nonconductive. Similar relations which map the conductivity of an $i$ order cell into the conductivity of an $i + 1$ order cell are now presented.

Figure 6 shows the various arrangements of conductive and nonconductive $i$ order cells which lead to conductive $i + 1$ order cells. The values in parentheses are the normalized conductivity of the arrangements and the number of arrangements having an identical normalized conductivity. The normalized conductivity of an arrangement is defined as the ratio of the flow through the arrangement to that which would be observed without obstructions. Hence, normalized conductivity is only a measure of the tortuosity imparted by flow obstructions. The normalized conductivity values were derived by applying the numerical models to the geometry of the arrangements using 30 × 30 and 20 × 20 × 20 arrays and by normalizing the resulting flow with respect to values computed for the array geometry without obstructions.

It is necessary to adopt a set of boundary conditions to apply to the arrangements in order to separate conductive and nonconductive arrangements and to define the normalized conductivities of the arrangements. The results shown in Table 1 and Figure 6 are based on the application of Dirichlet or first-type boundary conditions to the upper and lower surfaces of the arrangements and von Neumann or second-type boundary conditions to the lateral surfaces. This boundary condition configuration was adopted based on the observation that it leads to estimates of the critical probabilities which are consistent with values stated in the literature. As a result of the boundary condition configuration, there are topologically identical arrangements which are assigned different normalized conductivities. While counterintuitive, this condition is substantiated by verification studies presented herein.

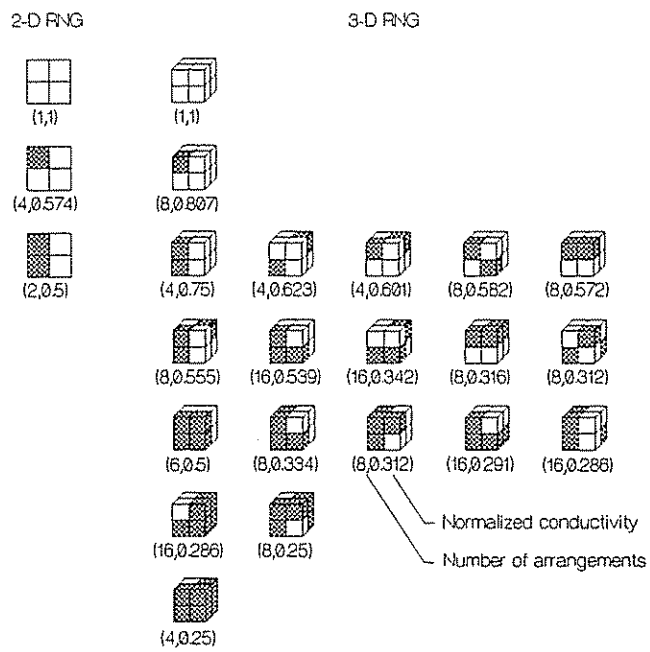


Fig. 6. Conductive $i + 1$ order arrangements of $i$ order cells. Nonconductive $i$ order cells are shaded.

Each normalized conductivity outcome, $k_j$, has a probability, $P_j$, which is a function of $p_i$. For example, the probability that a two-dimensional arrangement of cells has a normalized conductivity of 0.574 is

$$P = \frac{4p_i(1-p_i)^3}{1 - p_{i+1}} . \tag{8}$$

These probabilities are defined such that

$$\sum_{j=1}^{n} P_j = 1 \tag{9}$$

where n is the number of outcomes. From the definition of normalized conductivity, the arithmetic mean conductivity of $i + 1$ order cells is given by

$$K_{i+1} = K_i \sum_{j=1}^{n} P_j k_j , \tag{10}$$

the geometric mean conductivity by

$$K_{i+1} = K_i \prod_{j=1}^{n} k_j^{P_j} , \tag{11}$$

and the harmonic mean conductivity by

$$K_{i+1} = \frac{K_i}{\sum_{j=1}^{n} \frac{P_j}{k_j}} . \tag{12}$$

Equations (10)-(12) are plotted as a function of $p_i$ in Figure 7. The functions decrease from a value of unity for $p_i = 0$, where arrangements with no nonconductive $i$ order cells dominate, to 0.5 and 0.25 for $p_i = 1$, where arrangements with two and six nonconductive $i$ order cells dominate.

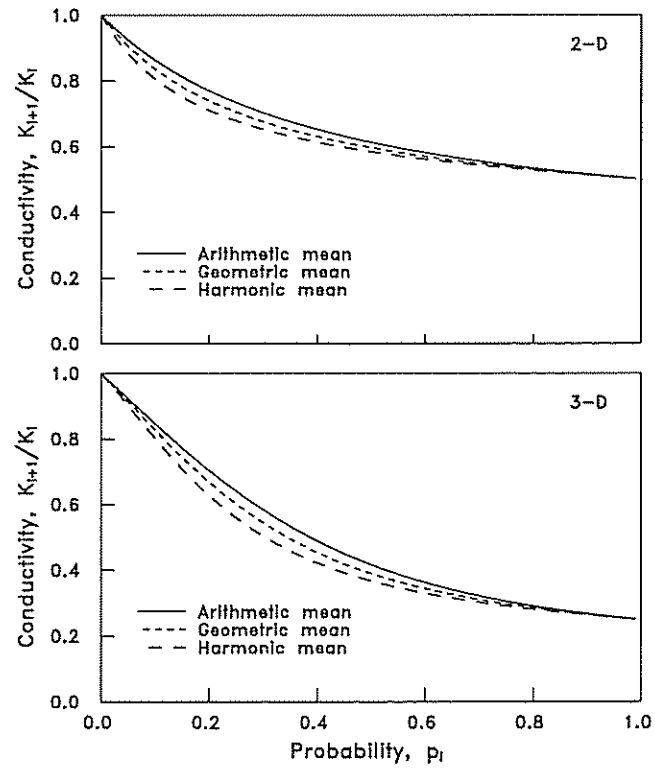


Fig. 7. Conductivity mapping functions relating the conductivities of $i$ and $i + 1$ order cells.

Figure 8 shows the results of iterating the geometric mean conductivity mapping function, (11), that is, calculating $p_1$ and $K_1$ from $p_o$ and $K_o$, $p_2$ and $K_2$ from $p_1$ and $K_1$, etcetera. The geometric mean conductivity mapping is presented because, as will be discussed in the following section, the geometric mean of a conductivity distribution yields the best estimate of bulk conductivity. The ratio of the conductivities of $i$ order to zero order cells, $K_i/K_o$, converges to a limit as the number of iterations approaches infinity with the limiting value equal to zero for $p_o > p_c$. The ratio $K_i/K_o$ may be interpreted as a tortuosity factor reflecting the influence of obstructions on the bulk conductivity of a domain.

Two series of experiments were performed in order to assess the validity of the conductivity mapping functions. The first series of experiments was performed using the numerical models and involved computing the normalized conductivity of the generated arrays as a function of zero order probability and scale. The modelling procedure follows from that described previously for the verification of the probability mapping function. The results of this study are compared to the conductivity mapping functions in Figure 8. Each point represents the average conductivity of the conductive outcomes observed during 20 runs. As zero order probability increases, the conductivities of the arrays decrease to approximately constant values which in turn decrease with increasing array size. This characteristic, which is also observed in the mapping functions, may be interpreted as a scale effect. There is general agreement between the numerical results and conductivity mapping functions; however, the numerical results are consistently less than the conductivity mapping functions, with the magnitude of the discrepancy increasing with increasing zero order probability. This tendency is largely the result of the excess tortuosity imparted by the finite difference approximation, which provides a poor approximation of the high gradients encountered in areas of flow constriction between obstructions. Consequently, the numerical results should not be expected to precisely match the conductivity mapping functions. The results can, however, be expected to support the trends predicted by the mapping functions.

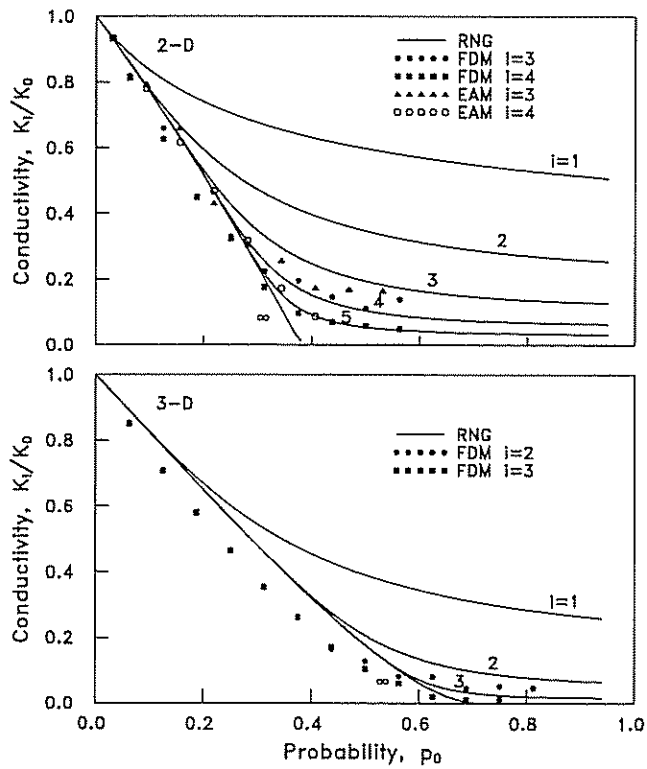


Fig. 8. Iterations of the geometric mean conductivity mapping functions. The conductivity mapping functions (RNG) are compared to data derived from the numerical models (FDM) and electrical analogue models (EAM).

The second series of experiments involved the use of electrical analogue models to provide an alternative comparison with the two-dimensional conductivity mapping. Electrical analogue models offer the advantage of being free from the excess tortuosity exhibited by the numerical models. Similar applications of electrical analogue models are reported by *Last and Thouless* [1971], *Shankland and Waff* [1974], *Sundaram and Frink* [1983], and *Chen et al.* [1989]. The experimental procedure followed is similar to the algorithm incorporated in the numerical model with the exception that nonconductive sites are represented by sequentially extracting sites from electrical analogue paper. Normalized conductivities are computed from measured electrical currents. Three 8 × 8 and three 16 × 16 arrays were studied. The data obtained from the experiments, averaged over the three replications of each array geometry, are shown in Figure 8 and compare very favorably with the mapping function. The scale effects observed for the numerical models and predicted by the mapping function are also apparent in the electrical analogue data.

## EXTENSION TO FINITE CONDUCTIVITY DISTRIBUTIONS

The derivation of the probability and conductivity mapping functions is based on the assumption that zero order cells are either conductive or nonconductive and, if conductive, have a characteristic conductivity. The central aspects of this assumption, namely, the definitions of conductive, nonconductive, and characteristic conductivity, warrant examination.

### *Bimodal Conductivity Distributions*

An operational definition of the term nonconductive is sought by examining the bulk conductivity of bimodal conductivity distributions as the minimum modal conductivity approaches zero relative to the maximum modal conductivity. A bimodal conductivity distribution is characterized by a minimum modal conductivity of $K_{min}$ which occurs with probability $p_{min}$ and by a maximum modal conductivity of $K_{max}$ which occurs with probability $p_{max} = 1 - p_{min}$.

*Bouwer* [1969] used resistor network electrical analogue models in an attempt to demonstrate that the bulk conductivity of a resistor network may be approximated by the geometric mean conductance of the individual elements. In one of the reported series of experiments, a bimodal distribution of resistors with conductances of $K_{min} = 1$ and $K_{max} = 10$ were randomly distributed on a 10 × 10 array. The relative proportions of the different resistors were varied, and the measured conductivity of the system was shown to be satisfactorily described by the geometric mean of the individual conductance values which is given by

$$\langle K \rangle_g = K_{\min}^{p_{\min}} K_{\max}^{1-p_{\min}}. \quad (13)$$

A modified version of this series of experiments was conducted using the numerical models. Bimodally distributed conductivities were assigned at random to each site in two- and three-dimensional 32 × 32 and 8 × 8 × 8 arrays, respectively. Four different conductivity distributions were examined, namely, $K_{max} = 1$ with $K_{min} = 10^{-1}$, $10^{-2}$, $10^{-3}$, and $10^{-4}$. The results of this study are shown in Figure 9, where each point represents the average bulk conductivity, $K_b$, observed for 20 runs. The geometric mean approximation to bulk conductivity, calculated using (13), would plot as a straight line in the semilogarithmic format of

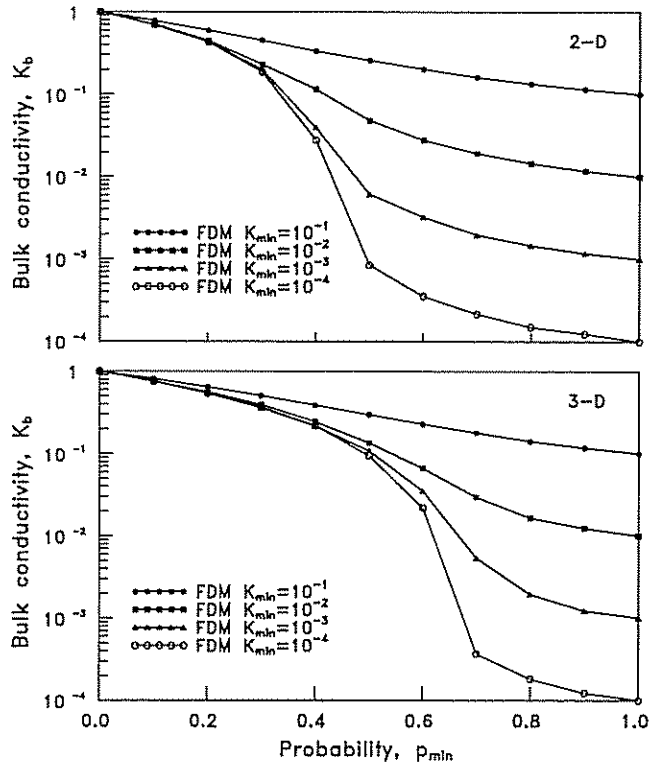


Fig. 9. Data derived from the numerical models for bimodal conductivity distributions with $K_{max} = 1$ and $K_{min} = 10^{-1}$, $10^{-2}$, $10^{-3}$, and $10^{-4}$.

Figure 9 and therefore satisfactorily describes the data for $K_{min} = 10^{-1}$. This conductivity distribution displays the same conductivity contrast ($K_{min}/K_{max} = 10^{-1}$) as that reported by *Bouwer* [1969]. The fidelity of the geometric mean approximation progressively degrades for $K_{min} = 10^{-2}$, $10^{-3}$, and $10^{-4}$. The data illustrate the onset of a percolation-like process as the value of $K_{min}$ approaches zero; that is, for $p_{min} < p_c$, $K_b$ becomes independent of the value of $K_{min}$ as the value approaches zero. It may therefore be concluded that the selection of modal conductivities of 1 and 10 by *Bouwer* [1969] was somewhat fortuitous relative to his substantiation of the geometric mean approximation to bulk conductivity. Clearly, the geometric mean approximation does not apply to bimodal conductivity distributions exhibiting a significant contrast in modal conductivity values.

The derivation of the conductivity mapping function is based on the assumption that the obstructed portions of a domain have a conductivity of zero. It is conceivable that the obstructions may have a small yet nonzero conductivity and, if this is the case, may be better characterized by $K_{min} << K_{max}$ than $K_{min} = 0$ where $K_{min}$ and $K_{max}$ are representative of the conductivities of the obstructed and unobstructed portions of the domain. As observed in Figure 9, $K_b$ converges to a limiting value as $K_{min}/K_{max}$ approaches zero for $p_{min} < p_c$. A limiting value is observed for $K_{min}/K_{max} < 10^{-2}$ over a large portion of the range $p_{min} < p_c$. This implies that the condition that a zero order cell is nonconductive may be interpreted as $K_{min}/K_{max} < 10^{-2}$ since continuing to decrease the value of $K_{min}$ does not produce a significant further decrease in $K_b$. The conductivity mapping function therefore remains valid provided that $K_{min}/K_{max} < 10^{-2}$ and $p_o < p_c$.

*Uniform Conductivity Distributions With Flow Obstructions*

A definition of the characteristic conductivity of zero order cells may be derived by the application of equivalent media theory which seeks to relate the bulk conductivity of a domain to a description of the distribution of conductivity within the domain. Numerous equivalent conductivity models have been introduced in the literature [*Warren and Price*, 1961; *Hashin and Shtrikman*, 1962; *Bouwer*, 1969; *Ambegaokar et al.*, 1971; *Madden*, 1976; *Gutjahr et al.*, 1978; *Berman et al.*, 1986]. The most commonly cited approximation relates bulk conductivity to the geometric mean of the statistical distribution of conductivity. This approximation has been repeatedly substantiated for spatially uncorrelated conductivity distributions. *Gutjahr et al.* [1978] demonstrated that the approximation also applies to spatially correlated conductivity distributions.

An intuitive argument may also be used to support the geometric mean approximation for bulk conductivity. A two- or three-dimensional arrangement of conductors is neither as sensitive to the presence of low-conductivity elements as a series arrangement of the conductors nor as sensitive to the presence of high-conductivity elements as a parallel arrangement. The conductivities of series and parallel arrangements of conductors are equal to the harmonic and arithmetic means of the individual conductivity values, $\langle K \rangle_h$ and $\langle K \rangle_a$, respectively. Bulk conductivity is therefore bounded by the harmonic and arithmetic means as described by

$$\langle K \rangle_h \leq K_b \leq \langle K \rangle_a . \tag{14}$$

The geometric mean, $\langle K \rangle_g$, of a conductivity distribution is similarly bounded by the harmonic and arithmetic means such that

$$\langle K \rangle_h \leq \langle K \rangle_g \leq \langle K \rangle_a . \tag{15}$$

A comparison of (14) and (15) leads to the conclusion that the geometric mean of a conductivity distribution may be used as a first order approximation of bulk conductivity; that is,

$$K_b \approx \langle K \rangle_g . \tag{16}$$

On the basis of the previous arguments, it is reasonable to assume that the characteristic conductivity of zero order cells may be approximated as the geometric mean of the conductivity of the cells. This notion is further examined by the recreation of the second series of experiments reported by *Bouwer* [1969]. In this series of experiments, resistors with conductances of 1-10 were assembled at random into $10 \times 10$ arrays, and the measured conductivities of the arrangements were shown to be favorably described by the geometric mean of the individual conductances.

To simulate this series of experiments using the numerical models, conductivities uniformly distributed in the range of $K_{min}$ to $K_{max}$ were assigned to each site in $32 \times 32$ and $8 \times 8 \times 8$ arrays. The geometric mean of a uniform conductivity distribution is

$$\langle K \rangle_g = e^{-1} K_{\max}^{\frac{K_{\max}}{K_{\max}-K_{\min}}} K_{\min}^{\frac{-K_{\min}}{K_{\max}-K_{\min}}} . \tag{17}$$

Four different conductivity distributions were examined, namely, $K_{min} = 1$ with $K_{max} = 10$, $10^2$, $10^3$, and $10^4$. Of particular interest is a means of treating systems which contain both conductive and nonconductive elements where the conductive elements display variable conductivity. Therefore, for each combination of $K_{min}$ and $K_{max}$, the proportion of nonconductive sites was varied between zero and 0.3 and zero and 0.7 for two- and three-dimensional systems, respectively. It should be noted that the presence of nonconductive sites is not factored into (17). The results of this study are shown in Figure 10, where each point represents the average bulk conductivity observed for 20 runs. It is suggested that the results may be approximated by the equivalent conductivity model

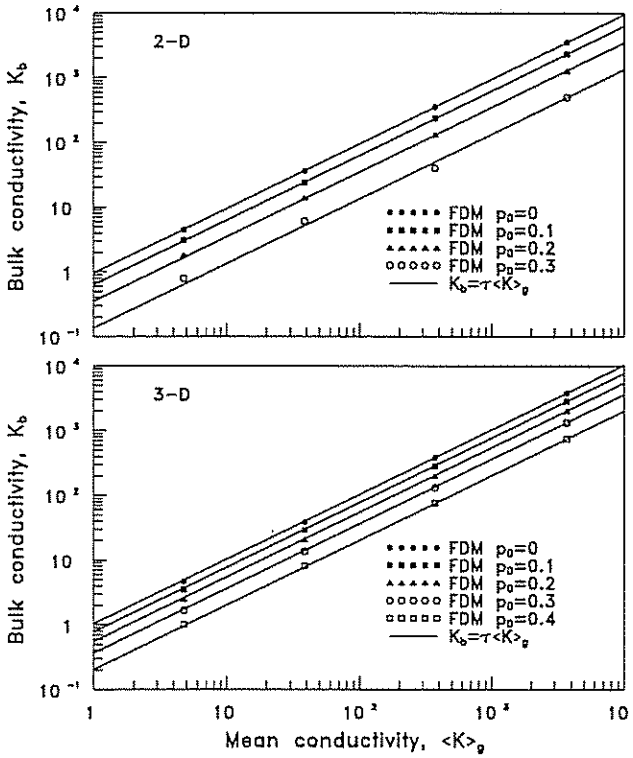


Fig. 10. Data derived from the numerical models for uniform conductivity distributions with $K_{min} = 1$ and $K_{max} = 10$, $10^2$, $10^3$, and $10^4$. The data (FDM) are compared to the equivalent conductivity model $K_b = \tau\langle K\rangle_g$.

$$K_b = \tau \langle K \rangle_g \tag{18}$$

where $\tau$ is a tortuosity factor related to the proportion of nonconductive sites. The solid lines shown in Figure 10 are the results of fitting (18) to the data using a least squares regression approach. Equation (18) appears to accurately describe the data, and therefore bulk conductivity may be estimated as the product of a tortuosity factor and geometric mean conductivity. A decoupling of the influences of flow obstructions and distributed conductivities is implied in this approximation. It is therefore assumed that the tortuosity imparted by flow obstructions is a function of the extent to which a domain is obstructed and is independent of the distribution of nonzero conductivities.

By definition, the tortuosity factor derived from the conductivity mapping function relates zero and $i$ order characteristic conductivities via

$$K_i = \tau\ K_o\ . \tag{19}$$

Bulk conductivity is analogous to $i$ order characteristic conductivity. Additionally, the tortuosity factors appearing in (18) and (19) are both solely functions of the proportion of zero order cells which are obstructed and therefore are equivalent. On the basis of these observations, it is concluded that the geometric mean conductivity of zero order cells may be used to represent the characteristic conductivity of zero order cells.

## Discussion and Conclusions

The probability and conductivity mapping functions, together with the experimentally defined relation for the proportion of a domain which is isolated from flow, are important results. Combined, these relations provide a basis for the description of flow through domains characterized by nonconductive inclusions where the term nonconductive implies a conductivity at least two orders of magnitude less than that of the unobstructed portion of the domain. The critical or percolation threshold obstruction densities derived from the probability mapping functions, defined as the maximum obstruction densities which will permit a continuous conduit to exist within a domain, are 0.382 and 0.718 for two- and three-dimensional flow, respectively. The influence of the obstructions on conductivity is derived from the conductivity mapping functions and expressed quantitatively as a tortuosity factor which varies from unity to zero as the density of obstructions varies from zero to the percolation threshold values. Bulk conductivity is then estimated as the product of the tortuosity factor and the geometric mean conductivity of the unobstructed portion of the domain. Flow is accommodated within the entire unobstructed portion of the domain for obstruction densities less than the percolation threshold values.

An important aspect of the mapping functions is the appearance of scale effects which are substantiated by the numerical and electrical analogue modelling results. The scale effects apparent in the probability mapping suggest that conductive domains may be encountered at obstruction densities greater than that corresponding to the percolation threshold value. The likelihood of such an occurrence decreases as the scale of the domain, relative to that of the obstructions, increases. Similarly, nonconductive domains may be encountered at obstruction densities less than the percolation threshold value. The scale effects apparent in the conductivity mapping function indicate that conductivity decreases with increasing domain scale and assumes a nonzero limiting value at obstruction densities less than the percolation threshold value and a value of zero at densities greater than the percolation threshold value. These scale effects have implications in the extrapolation of physical properties measured at conventional laboratory and in situ scales to the scale of relevant geologic processes.

The simplicity of the models introduced in this paper is achieved at the cost of adopting highly idealized representations of the spatial distribution of obstructions and conductivity and of accepting statistical, rather than deterministic, estimates of behavior. The assumption of isotropic behavior is also an acknowledged limitation. A compromise between the simplicity of these and other analytical models and the need to accurately represent the structure of geologic features must be established. While the models introduced in this paper are simple in form, it is suggested that simple models which capture the essential physics of geologic processes will frequently prove to be adequate, particularly in light of the limitations of subsurface reconnaissance techniques.

*Acknowledgments.* Funding for this research was provided by the United States National Science Foundation under award numbers MSM-8611249 and MSM-8708976 and by the Department of Mineral Engineering of the Pennsylvania State University. The support of these institutions is gratefully acknowledged.

## References

Allègre, G.J., J.L. Le Mouel, and A. Provost, Scaling rules in rock fracture and possible implications for earthquake prediction, *Nature, 297*, 47-49, 1982.

Ambegaokar, V., B.I. Halperin, and J.S. Langer, Hopping conductivity in disordered systems, *Phys. Rev. B, 4*, 2612-2620, 1971.

Atkinson, K.E., *An Introduction to Numerical Analysis*, John Wiley, New York, 1978.

Berman, D., B.G. Orr, H.M. Jaeger, and A.M. Goldman, Conductances of filled two-dimensional networks, *Phys. Rev. B, 33*, 4301-4302, 1986.

Bouwer, H., Planning and interpreting soil permeability measurements, *J. Irrig. Drain. Div. Am. Soc. Civ. Eng., 95*, 391-402, 1969.

Charlaix, E., E. Guyon, and N. Rivier, A criterion for percolation threshold in a random array of Plates, *Solid State Commun., 50*, 999-1002, 1984.

Chelidze, T.L., Percolation and fracture, *Phys. Earth Planet. Inter., 28*, 93-101, 1982.

Chen, D.W., R.W. Zimmerman, and N.G.W. Cook, The effect of contact area on the permeability of fractures, in *Proceedings of the 30th U.S. Symposium on Rock Mechanics*, pp. 81-88, A.A. Balkema, Rotterdam, 1989.

de Marsily, G., Flow and transport in fractured rocks: Connectivity and scale effect, in *Memoirs of the 17th International Congress of the International Association of Hydrogeologists*, vol. XVII, part 1, pp. 267-277, International Association of Hydrogeologists, Tucson, Az., 1985.

Dienes, J.K., Permeability, percolation and statistical crack mechanics, in *Proceedings of the 23rd U.S. Symposium on Rock Mechanics*, pp. 86-94, Port City Press, Baltimore, Md., 1982.

Gentier, S., and D. Billaux, Caractérisation en laboratoire de l'espace fissural d'une fracture, in *Proceedings of the International Symposium on Rock at Great Depth*, vol. 1, pp. 425-431, A.A. Balkema, Rotterdam, 1989.

Golden, J.M., Percolation theory and models of unsaturated porous media, *Water Resour. Res., 16*, 201-209, 1980.

Gueguen, Y., and J. Dienes, Transport properties of rocks from statistics and percolation, *Math. Geol., 21*, 1-13, 1989.

Gutjahr, A.L., L.W. Gelhar, A.A. Bakr, and J.R. MacMillan, Stochastic analysis of spatial variability in subsurface flows, 2, Evaluation and application, *Water Resour. Res., 14*, 953-959, 1978.

Hashin, Z., and S. Shtrikman, A variational approach to the theory of the effective magnetic permeability of multiphase materials, *J. Appl. Phys., 33*, 3125-3131, 1962.

Hestir, K., and J.C.S. Long, Analytical expressions for the permeability of random two-dimensional Poisson fracture networks based on regular lattice percolation and equivalent media theories, *J. Geophys. Res., 95*, 21565-21581, 1990.

Kirkpatrick, S., Percolation and conduction, *Rev. Mod. Phys., 45*, 574-588, 1973.

Last, B.J., and D.J. Thouless, Percolation theory and electrical conductivity, *Phys. Rev. Lett., 27*, 1719-1721, 1971.

Madden, T.R., Random networks and mixing laws, *Geophysics, 41*, 1104-1125, 1976.

Madden, T.R., Microcrack connectivity in rocks: A renormalization group approach to the critical phenomena of conduction and failure in crystalline rocks, *J. Geophys. Res., 88*, 585-592, 1983.

Piggott, A.R., Analytical and experimental studies of rock fracture hydraulics, Ph.D. thesis, Pennsylvania State Univ., University Park, Pa., 1990.

Pyrak-Nolte, L.J., L.R. Myer, N.G.W. Cook, and P.A. Witherspoon, Hydraulic and mechanical properties of natural fractures in low permeability rock, in *Proceedings of the 6th International Congress on Rock Mechanics*, vol. 1, pp. 225-231, A.A. Balkema, Rotterdam, 1987.

Robinson, P.C., Connectivity of fracture systems - A percolation theory approach, *J. Phys. A Math. Gen., 16*, 605-614, 1987.

Shankland, T.J., and H.S. Waff, Conductivity in fluid bearing rocks, *J. Geophys. Res., 79*, 4863-4868, 1974.

Shante, V.K.S., and S. Kirkpatrick, An introduction to percolation theory, *Adv. Phys., 20*, 325-357, 1971.

Smalley, R.F. Jr., D.L. Turcotte, and S.A. Solla, A renormalization group approach to the stick-slip behavior of faults, *J. Geophys. Res., 90*, 1894-1900, 1985.

Sundaram, P.N., and D. Frink, Electrical analogy of hydraulic flow through rock fractures, *Geotech. Test. J., 6*, 3-6, 1983.

Sykes, M.F., and J.W. Essam, Critical percolation probabilities by series methods, *Phys. Rev., 133*, A310-A315, 1964.

Turcotte, D.L., Fractals and fragmentation, *J. Geophys. Res., 91*, 1921-1926, 1986.

Warren, J.E., and H.S. Price, Flow in heterogeneous porous media, *Soc. Pet. Eng. J., 1*, 153-169, 1961.

Wilke, S., E. Guyon, and G. de Marsily, Water penetration through fractured rocks: Test of a tridimensional percolation description, *Math. Geol., 17*, 17-27, 1985.

D. Elsworth, Department of Mineral Engineering, Pennsylvania State University, 104 Mineral Sciences Building, University Park, PA 16802.

A. R. Piggott, National Water Research Institute, 867 Lakeshore Road, Burlington, Ontario, L7R 4A6.

(Received April 12, 1991;
revised August 29, 1991;
accepted October 17, 1991.)